Neutralization of slow multicharged ions at a clean gold surface: Total electron yields

H. Kurz, F. Aumayr, C. Lemell, K. Töglhofer, and HP. Winter
Institut für Allgemeine Physik, Technische Universität Wien, Wiedner Hauptstraße 8-10/134, A-1040 Wien, Austria
(Received 21 December 1992)

Total slow-electron ($E_e \leq 60$ eV) yields as derived from measured electron-emission statistics are presented for impact of various slow ($v_p \leq 10^5$ m/s) multicharged ions (N^{5+},N^{6+},Ne^{5+}–Ne^{10+}, Ar^{5+}–Ar^{16+}, Kr^{5+}–Kr^{10+}, Xe^{6+},Xe^{8+},Xe^{10+}, and I^{16+},I^{20+},I^{23+},I^{25+}) on atomically clean polycrystalline gold. The experimental data can successfully be modeled by classical over-barrier-type calculations, in which way three different electron-emission processes have been identified, i.e., autoionization of the transiently neutralized projectile ("hollow atom") on its approach toward the surface, promotion into vacuum of electrons captured by the projectile, and "peeling off" of electrons remaining bound in highly excited states until projectile impact on the surface. The relative importance of these three processes depends strongly both on projectile species and impact velocity.

PACS number(s): 79.20.Nc, 31.50.+w, 79.90.+b

I. INTRODUCTION

Production and decay of so-called hollow atoms has become a most interesting topic in the field of ion-surface interactions. Such highly inverted, multiexcited atoms can be formed by fast resonant neutralization (RN) during the approach of slow ($v \ll 1$ a.u.) multicharged ions (MCI's) toward a metal surface. The first evidence for the existence of hollow atoms near a surface has been found from the analysis of the resulting soft-x-ray emission ($K\alpha$ satellites) [1,2] and fast-Auger-electron emission [3–5] in the course of MCI-surface collisions.

The formation of hollow atoms near a surface can be studied in several ways, e.g., by analyzing the resulting total electron emission [6,7], the ejected electron energy distributions [4,5,8–13], the reflected ion charge states [14,15] and angular distributions [15,16] and the emission of soft x rays [1,2,10,17,18]. The observed electron energy distributions are dominated by broad low-energy continua ($E_e < 30$ eV) [8,19,20] with some much smaller contributions from fast Auger electrons [4,5,9–13, 19–21]. Several reviews on the interaction of slow MCI's with surfaces [10,22–24] are available and related semiclassical [25] and classical [26] calculations have recently been conducted. In addition, some quantum-mechanical calculations on the involved resonant neutralization or ionization (RN or RI) [27] and autoionization (AI) [28] processes have been made.

The now widely accepted scenario for a slow MCI approaching a metal surface consists of resonant neutralization of the projectile by capturing electrons from the metal conduction band near the Fermi edge, followed by deexcitation in small energy steps (auto-ionization cascades). Taking a closer look, however, the following questions may be asked:

Are there other mechanisms, besides autoionization, which can produce the observed slow electrons? There is some evidence that AI processes alone cannot be responsible for the observed velocity-dependence of the total electron emission yields [29].

When, where, and how do the inner-shell vacancies decay which have been formed during the projectile's approach towards the surface?

Finally, what happens on the outgoing part of the trajectory of a scattered hollow atom?

In the following, a study is presented on slow-electron-emission yields resulting from impact of slow MCI's on a clean gold surface, which have been derived from measured electron-emission statistics (ES), i.e., the distribution of probabilities W_n for emission of $n=0,1,2,\ldots$ electrons due to the impact of individual projectiles on the surface. Some of these results for Ar^{q+} ions ($q \leq 16$) have already been published but only interpreted in a qualitative way [29]. Section II contains a detailed description of our experimental setup and data evaluation procedure, and in Sec. III we present sets of total electron yields for Ar ions ($q \leq 16$) as well as for N^{q+} ($q=5,6$), Ne^{q+} ($q \leq 10$), Kr^{q+} ($q \leq 10$), Xe^{q+} ($q=6,8,10$), and I^{q+} ($q=16,20,23,25$). A quantitative interpretation of all related data on the basis of an extended classical over-the-barrier model [25] will be given in Sec. IV.

In the present paper only the total-electron-emission yields will be considered, but further useful information can be deduced from the measured electron-emission statistics themselves, as will be shown in a companion paper. Atomic units are used unless otherwise stated.

II. EXPERIMENTAL SETUP AND DATA EVALUATION

The multicharged ions applied in this study have been produced by a recoil ion source [30] in the following way. Fast-heavy-ion beams (3–11 MeV/amu) from the GSI UNILAC accelerator (Darmstadt, Germany) have been directed through suitable gas or vapor targets. The resulting slow, highly ionized recoil ions were extracted by a small potential difference (about 2 V) and subsequently accelerated by a few hundred volts and charge-to-mass separated in a 180° magnet. After passing a differentially pumped drift region of ca. 1 m the ions could be either

further accelerated or decelerated by a four-cylinder lens assembly, before hitting the target surface under normal incidence. The rather small spread in initial kinetic energy of the recoil ions [31] gave access to "nominal" (see below) final impact energies as low as $E_{\rm kin} \geq (2\pm1)q$ eV (q being the projectile ion charge). Typical ion fluxes at the target surface were, e.g., 10^4 Ar^{10+} or 10^2 Ar^{16+} ions/s. All electrons ejected from the target with energies $E_e \leq 60$ eV into the full 2π solid angle were deflected by a highly transparent (96%) conical electrode and then, after extraction from the target region, accelerated and focused onto a surface barrier detector (Canberra PD 100-12-300 AM) connected to +26 kV with respect to the target [32]. Figure 1 shows a sketch of the last section of the deceleration-target-detector unit with typical primary ion—as well as ejected electron trajectories. In this particular example, the potentials of the various parts have been set in order to decelerate ions Z^{q+} from an initial kinetic energy of $400q$ eV down to Uq eV, and at the same time to extract the emitted electrons towards the solid-state detector.

The target (polycrystalline gold) was regularly sputter cleaned [33] with a built in 2-keV Ar^+-ion gun. By means of a turbomolecular pump, a Ti-sublimation pump and liquid-nitrogen-cooled baffle the whole deceleration-target-detector assembly was kept in UHV at a base pressure below 3×10^{-8} Pa during all measurements.

All electron emission events induced by an individual impinging projectile particle will be finished within less than 10^{-11} s [24], which is much shorter than the resolution time of the applied detection electronics ($\geq 10^{-6}$ s). Thus, n electrons emitted due to impact of one projectile are registered like *one* electron of $n\times26$ keV rather than a number n of 26-keV electrons. Consequently, the area below the nth peak of the resulting electron "energy" spectra is directly related to the probability W_n for emission of n electrons. Equation (1) gives the relation between the individual probabilities W_n and the total-electron-emission yield γ (i.e., the mean number of electrons emitted due to impact of one projectile):

$$\gamma = \sum_{n=1}^{\infty} nW_n \ , \quad \sum_{n=0}^{\infty} W_n = 1 \ . \tag{1}$$

The probability W_0 that no electron is emitted cannot be determined directly, but may practically be neglected for yields $\gamma \geq 3$. Electrons which are reflected from the

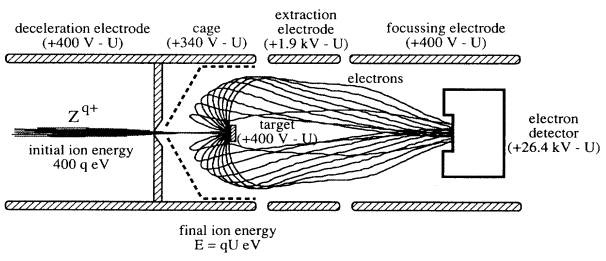

FIG. 1. Setup for measuring statistics of ion-induced electron emission for impact of slow ($E_{\rm kin} \geq 2q$ eV) highly charged ions on a clean gold target. Indicated potentials refer to deceleration of a beam of ions Z^{q+} from $400q$ eV down to a final kinetic energy of Uq eV on the target.

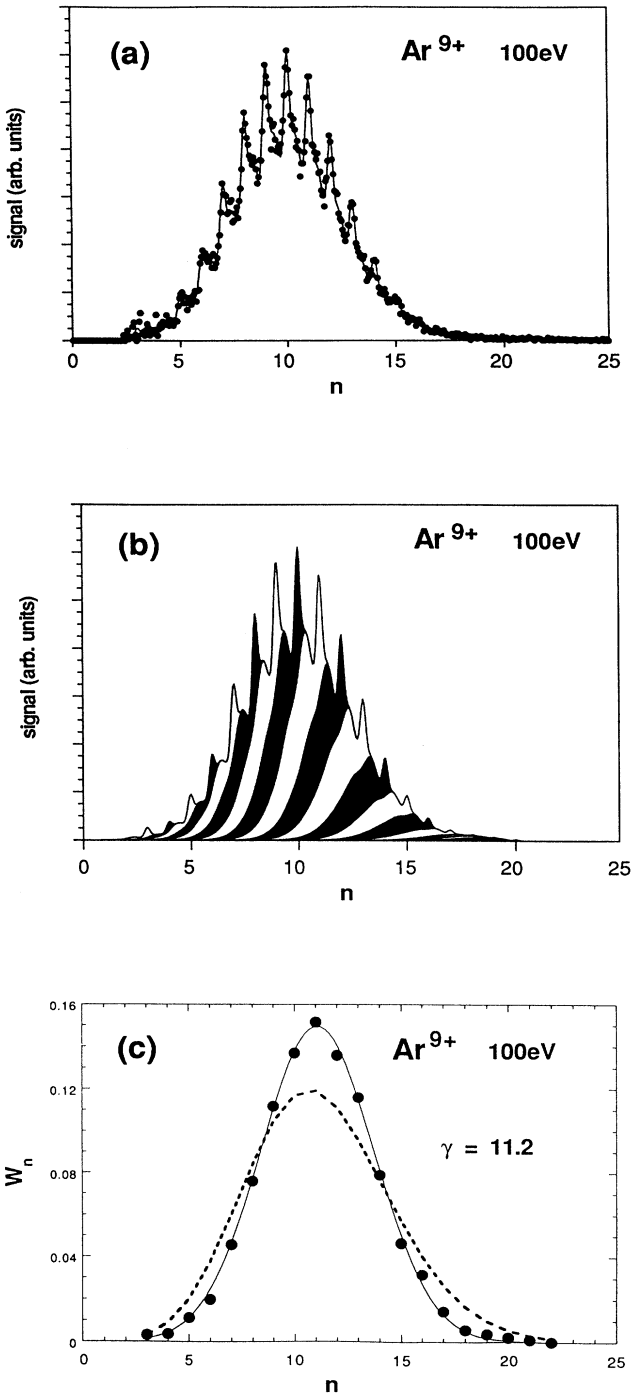

FIG. 2. (a) Measured pulse height spectrum for impact of 100 eV Ar^{9+} ($v_p \approx 2.2\times10^4$ m/s) on gold (full symbols) and corresponding fit (solid line) taking account of electron backscattering from the detector surface. (b) Fit to the above spectrum shown as a sum of contributions for emission of 1,2,3, . . . electrons. Contributions related to probabilities for the emission of even numbers of electrons are shaded for guidance. The area of the nth "stripe" is equal to the probability W_n in Eq. (1). (c) Probability distribution W_n resulting from this fitting procedure. The solid line is a Gaussian distribution fitted to the W_n, whereas the dashed line is a Poissonian distribution with the same mean value γ.

detector surface (fraction $\approx 15\%$ [34]) will deposit only part of their kinetic energy in the detector and thus add to the simple Gaussian peak shapes [a full width at half maximum (FWHM) of approximately 6 keV] a broader structure [35] of well-known shape [36,37] on the low-energy side of each peak. These structures become dominant for peaks corresponding to higher numbers of electrons [cf. Fig. 2(b)]. A least-squares fit of a linear combination of such peak shapes to the measured pulse height spectra [Fig. 2(b)] delivers the emission probability distributions W_n [Fig. 2(c)], from which the total electron yields can then be obtained directly via Eq. (1).

III. EXPERIMENTAL RESULTS

As described above, we have measured ES to derive from them the total slow electron emission yields for the projectile species N^{5+},N^{6+},Ne^{5+}–Ne^{10+}, Ar^{5+}–Ar^{16+}, Kr^{5+}–Kr^{10+}, Xe^{6+},Xe^{8+},Xe^{10+}, and I^{16+},I^{20+},I^{23+}, I^{25+} impinging on clean gold. The nominal (see below) kinetic energy of these projectiles was varied between typically $2q$ eV and $400q$ eV, and the resulting total slow-electron yields γ have been plotted versus projectile velocity v_p in Figs. 3 and 4. For the moment, the solid lines which represent fits according to Eq. (2) [29] are only meant for guidance:

$$\gamma(v_p)=\frac{C_1}{\sqrt{v_p}}+\gamma_\infty \ . \tag{2}$$

In Table I total electron emission yields γ for three selected impact velocities have been collected, and in the last column the velocity-independent fitting parameter γ_∞ has been added.

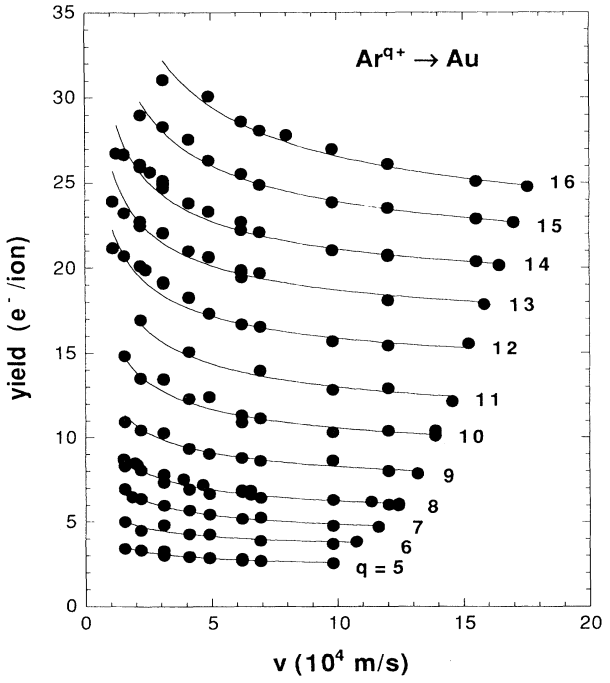

FIG. 3. Measured total electron yields vs impact velocity v_p for Ar^{q+} ions impinging on clean gold.

Already on first sight, the following general trends are obvious:

Within the charge-state manifold of each projectile species the yields γ increase with q, but decrease with increasing projectile velocity, and consequently level off at high impact velocity towards apparently constant values γ_∞ [cf. Eq. (2)]. For projectile velocities up to 2×10^5 m/s the kinetic emission yields for the respective singly and doubly charged ions remain well below 0.5 electrons/ion [32,38] and thus cannot be responsible for the just-mentioned leveling-off behavior.

The total electron yield for impact of I^{25+}, which was the highest charged ion accessible to us thus far, varies from 40 up to 70 electrons per incoming ion, whereas for fully stripped (Ne^{10+}) and hydrogenlike ions (N^{6+} and Ne^{9+}) almost constant yields over the whole impact-velocity range can be observed.

In Fig. 5(a) electron yields have been plotted versus the total potential energy $W_{q,\mathrm{pot}}$ carried by ions Ar^{q+} (closed symbols, $v_p \approx 4.9\times 10^4$ m/s). $W_{q,\mathrm{pot}}$ is defined as

$$W_{q,\mathrm{pot}}=\sum_{i=1}^{q} W_{i-1\rightarrow i} \ , \tag{3}$$

where $W_{i-1\rightarrow i}$ is the ionization potential of $Z^{(i-1)+}$, i.e., the energy needed to remove one electron from the ion $Z^{(i-1)+}$. These ionization potentials have been calculated by using Slater's rules [39], and are equal within 5% to the sum of ionization potentials of the corresponding ground state ions given by Kelly and Palumbo [40]. As has been noted by different authors [7,8,11] for charge states $q \leq 8$ the yields $\gamma(q)$ remain directly proportional to the corresponding values $W_{q,\mathrm{pot}}$. In Fig. 5(a), the slope of the dashed line fitted to the γ values for $q \leq 8$ corresponds to an average energy of 80 eV needed for emission of one slow electron. For $q \geq 10$ the yields may again be approximated by a straight line, which now, however, corresponds to a "cost" of about 250 eV for emitting each additional electron. Ar ions of charge states $q \leq 8$ have completely filled K and L shells, whereas for $q > 8$ an increasing number of L-shell vacancies will show up. Assuming that the RN-AI deexcitation cascades do not find enough time to fill these vacancies before the projectiles reach the surface (i.e., Auger transitions into the L shell have practically not yet taken place, cf. also Refs. [5,10,13]), they will reach the surface with about q electrons in the M shell and/or higher shells, and still $(q-8)$ vacancies in the L shell. Consequently, the potential energy of such a $(q-8)$-fold highly excited atom has not yet been made available for emission of slow electrons in the RN-AI cycle. Plotting the observed total yields γ versus the remaining ("usable") potential energy [open symbols in Fig. 5(a)] indicates that the proportionality of γ with potential energy as obtained for $q \leq 8$ is continued also for $q > 8$ up to the highest charge states investigated if only this usable potential energy is considered.

In Fig. 5(b) we compare the dependence of slow-electron yields on $W_{q,\mathrm{pot}}$ for Ne, Ar, and Kr ions of equal velocity $v_p \approx 4.9\times 10^4$ m/s. For both Ne and Ar projectiles the additional potential energy carried by inner-shell vacancies in the case of charge states $q > 8$ (K-shell vacancies for Ne^{q+}, L-shell vacancies for Ar^{q+}), where the

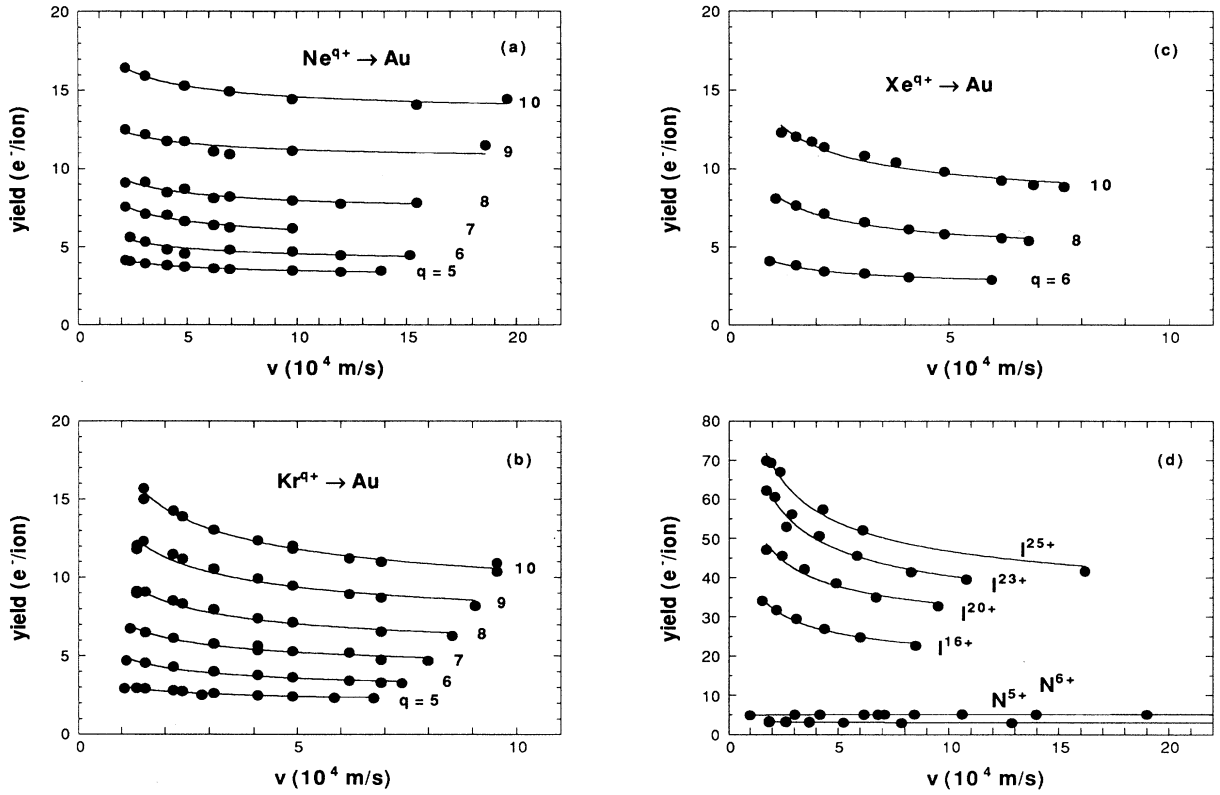

FIG. 4. Measured total electron yields vs impact velocity v_p for (a) Ne^{q+}, (b) Kr^{q+}, (c) Xe^{q+}, and (d) N^{q+} and I^{q+} ions impinging on gold.

steps between neighboring levels become relatively large, is obviously much less efficient for electron emission than the potential energy of ions in charge states $q \leq 8$. For Kr^{5+}–Kr^{10+}, where both K and L shells are still intact, there is much less change of the γ vs $W_{q,\mathrm{pot}}$ relationship when proceeding beyond $q=8$. Furthermore we observe that for the lower charge states $q \leq 8$ the γ vs $W_{q,\mathrm{pot}}$ curve is less steep for Ne (corresponding to ≈ 110 eV potential energy for emitting one electron), than for Ar (≈ 80 eV/electron) and Kr (≈ 70 eV/electron), respectively. Again, the potential energy of the projectile ion seems to be usable for slow electron emission via AI processes the more efficient the smaller the energy steps between neighboring projectile levels. This last finding shows that in contrast to earlier belief [8] also for projectiles without inner-shell vacancies, not only the total potential energy, but also the electronic structure of the projectile will influence the resulting slow electron yields.

A more detailed investigation of Ar^{q+} results reveals the surprising fact, that for $q > 8$ the total electron yields increase practically linearly with q, as illustrated in Fig. 6 for two different nominal velocities and the velocity-independent fitting parameter γ_∞.

To estimate the experimental errors of our γ data, the following considerations are of interest. Most projectiles backscattered from the target will leave the cage around the target in the neutral state, but some of them may hit the cage wires and thus produce additional electrons. Considering the reflection coefficient of slow heavy particles from gold (typically $<50\%$ [41]), the transparency of the cage mesh (96%) and the comparably small electron emission yields for slow neutral and singly charged projectiles (<0.5 electrons/ion) we estimate the contribution of these additional electrons to the total yields to be less than 1%. Careful measurements and ray-tracing calculations demonstrated that more than 97.5% of the electrons emitted from the target with energies less than 60 eV will reach the sensitive area of the detector. Emission of fast Auger electrons in the processes studied can be neglected as far as the results presented here are concerned. Evaluation of the measured data by the fitting procedure described above may cause additional systematic errors ($\pm 2\%$). The overall uncertainty for the total slow electron yields reported above is therefore estimated to be about $\pm 4\%$.

The kinetic energy distribution of the impinging projectiles is broadened by the potential drop across the ionization volume in the recoil ion source ($\Delta E \leq q$ eV), the initial kinetic energy spread of the recoil ions (<1 eV for noble-gas ions [31] as well as for I ions produced from HI, ~ 50 eV for N^{5+} and N^{6+} produced from N_2), and some errors in measuring the potentials applied to target and ion source, respectively. With the exception of N^{q+} ($q=5,6$) projectiles, where in the regarded impact velocity range the electron emission yield apparently does not change at all, at the lowest kinetic energies ($\approx 2q$ eV) the uncertainty of the nominal projectile velocity will be about 25%, but at e.g., $10q$ eV already less than 5%.

The interaction of an ion with its image charge will accelerate the projectile toward the surface, thus resulting in a gain in kinetic energy of the order of $\Delta E_{q,\mathrm{im}} \approx q^{3/2}$ eV [15,16,29]. For slow projectiles ($E_{\mathrm{kin}} < 100$ eV) in high charge states ($q \geq 15$), $\Delta E_{q,\mathrm{im}}$ may even exceed the initial kinetic energy and the actual impact velocity will then be increased by up to a factor of 1.5. Throughout this paper the terms "nominal" kinetic energy and "nominal" projectile velocity refer to the value without image charge acceleration taken into account. The deviation of the data points at low impact energies from the fitted curves for higher charge states of Ar^{q+} in Fig. 3 may be related to the just explained gain in projectile velocity due to image charge attraction.

IV. DISCUSSION OF EXPERIMENTAL RESULTS IN COMPARISON WITH MODEL CALCULATIONS

In order to describe the neutralization and deexcitation processes of MCI's during their interaction with a metal surface, we have applied a classical over-the-barrier model (CBM) first presented in Ref. [25]. The main assumptions of this model (for a more detailed description the reader is referred to [25]) are the following.

During the approach of a MCI (charge state q) toward a metal surface (decreasing ion-surface distance R), at a critical distance $R_c(q)$

$$R_c(q) = \frac{1}{2W_\Phi}\sqrt{8q+2} \tag{4}$$

TABLE I. Total electron emission yields γ for impact velocities $v_p = 2.2\times10^4$ m/s, 4.9×10^4 m/s, and 9.8×10^4 m/s, respectively. γ_∞ is the velocity-independent fitting parameter obtained from Eq. (1).

		Total yields $\gamma(v_p)$			
Projectile \ v_p (10^4 m/s)	q	2.2	4.9	9.8	γ_∞
N	5	3.0	3.0	3.0	2.9
	6	5.0	5.1	5.0	5.0
Ne	5	3.7	3.6		2.9
	6	4.8	4.7		3.7
	7	6.7	6.2		4.8
	8	8.7	8.2		6.8
	9	12	11		10
	10	15	15		13
Ar	5	3.3	2.9	2.5	2.0
	6	4.5	4.2	3.7	3.0
	7	6.4	5.4	4.7	3.5
	8	8.1	6.7	6.3	4.7
	9	10	9.0	8.6	6.4
	10	13	12	10	7.8
	11	14	13		9.4
	12	20	17	16	13
	13	22	21		16
	14	26	23	21	18
	15	26	25		19
	16	27			20
Kr	5	2.8	2.4		1.9
	6	4.3	3.6		2.4
	7	6.1	5.3		3.6
	8	8.5	7.1		4.6
	9	11	9.5		6.2
	10	14	12		7.4
Xe	6	3.5			2.1
	8	7.1	5.8		3.7
	10	11	9.8		6.7
I	16	31	26		16
	20	45	38	33	22
	23	61	47	40	24
	25	68	55	47	29

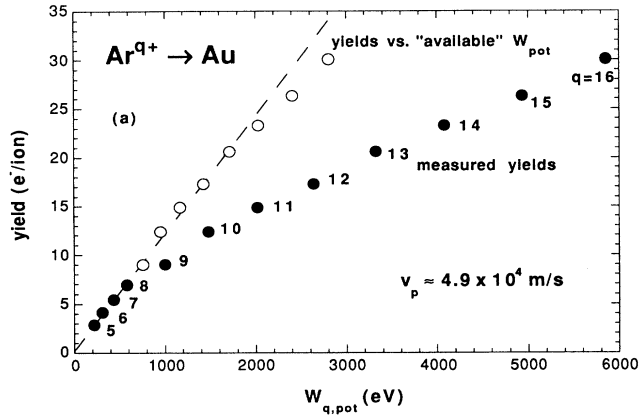

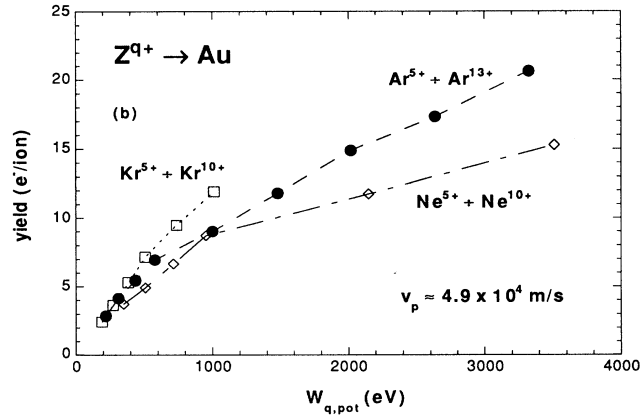

FIG. 5. (a) Measured total slow electron yields vs total potential energy (full symbols) and "usable" potential energy (open symbols), respectively, for 500 eV Ar ions ($v_p \approx 4.9 \times 10^4$ m/s) impinging on clean gold. (b) Total electron yields vs potential energy for Ne^{q+} (diamonds), Ar^{q+} (full circles), and Kr^{q+} (squares) ions impinging on clean gold ($v_p \approx 4.9 \times 10^4$ m/s).

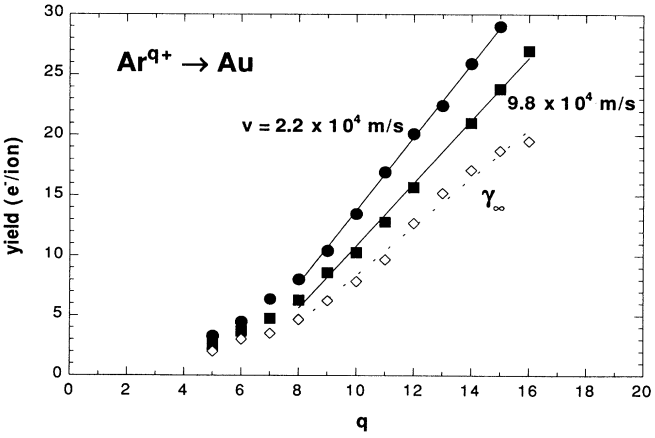

FIG. 6. Measured total electron yields and fitting parameter γ_∞ [cf. Eq. (1)] vs charge state q for Ar^{q+} ions impinging on clean gold with different impact velocities.

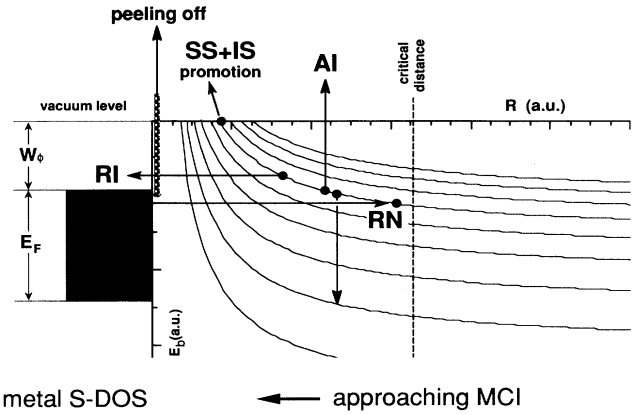

FIG. 7. States of a neutralizing multicharged ion approaching a metal surface. All processes considered in the model calculations are indicated. Electrons captured via RN can be emitted via AI, promotion into vacuum due to screening and image shift (SS+IS), and "peeling off" those electrons, which cannot exist inside the solid. Furthermore, recapturing of electrons into the solid via RI can take place. (S-DOS, surface density of states.)

(W_Φ is the work function of the metal), the potential barrier acting upon an electron of the height

$$V = -\frac{1}{2R}\sqrt{8q+2}\ , \tag{5}$$

formed by the projectile's potential, its image potential, and the image potential of the electron to be captured is decreased below the Fermi level of the metal. Consequently, at R_c the ion can start to capture electrons resonantly from the conduction band (resonant neutralization, RN) into highly excited projectile states (cf. Fig. 7). This RN stops as soon as the captured electrons decrease the ion charge state q and, as a consequence, the potential barrier will rise again above the Fermi level. With further approach, the condition $R \leq R_c(q)$ can again be satisfied and RN will continue. In parallel with the RN, Auger processes can promote electrons bound on the projectile either above the vacuum level (AI) or into empty states above the Fermi level of the conduction band ("Auger-loss to conduction band," AL).

The projectile energy levels are shifted upwards due to (a) interaction with the image charge of the ion core ("image shift," IS) and (b) screening of the charge of the ion core by electrons already occupying lower levels due to previous RN-AI processes ("screening shift," SS) [10,25].

Electrons that are shifted above the potential barrier and the Fermi level, can of course be lost again in empty states of the conduction band (resonant ionization, RI). Since the AI-related electron yield should decrease with increasing projectile velocity (i.e., decreasing flight time from the critical distance R_c to the target surface), AI cannot account for the velocity-independent part γ_∞ of the measured yields (cf. Sec. III). Therefore other emission mechanisms have to be responsible for this contribution. Two promising candidates for such mechanisms have been mentioned in Ref. [25] and have therefore been introduced into our model calculations. On the one hand, electrons "surviving" AI and RI can be promoted

above the vacuum level and thus escape ("IS+SS promotion"). On the other hand, as soon as the hollow atom strikes the surface, a third electron-emitting process should become operative. The still populated outer shells of such a projectile are "peeled off" (PO), because of dynamical screening inside the solid [25,42]. Our model considers an electron to be peeled off, if its corresponding Bohr radius $r_B = n^2/q$ at the moment of projectile impact on the surface is still larger than the screening length for surface plasmons $\lambda_s = v_F/\omega_p$ of the metal (v_F is the Fermi-velocity; ω_p is the surface plasmon frequency; in the case of a gold target, $\lambda_s \approx 3$ a.u.).

Energy levels of bound electrons have been calculated by assuming hydrogenlike states and using Slater's rules to account for screening of the respective nuclear charge [39]. Subshell effects have been neglected, however.

With all the above described assumptions, a set of coupled rate equations [25] can be obtained for the populations P_n of the nth shells of the projectile as a function of its distance from the surface, plus two further equations for the number of autoionized electrons and electrons promoted into vacuum due to SS+IS, respectively. In addition, Newton's equation of motion governs the evolution of the perpendicular velocity of the projectile under the influence of its image charge. As an example, Fig. 8 illustrates such a modeled evolution for Ar^{12+} ions impinging on clear gold ($W_\Phi = 5.1$ eV) with a nominal kinetic energy of 750 eV ($v_p \approx 6\times10^4$ m/s), exposing the following development.

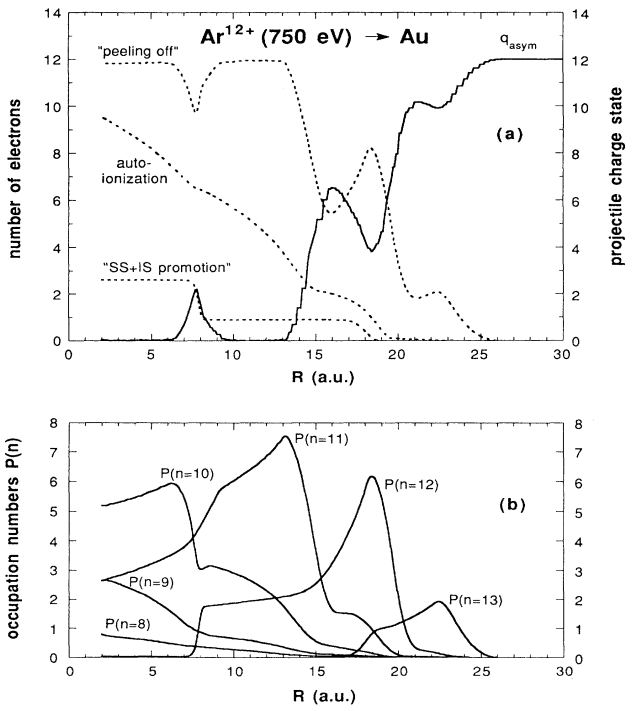

FIG. 8. Modeled neutralization of a 750 eV Ar^{12+} ion ($v_p \approx 6\times10^4$ m/s) approaching a gold surface: (a) Evolution of ion charge state q, number of emitted electrons (autoionization and promotion), and number of electrons that will be emitted (peeling off) when the projectile hits the surface vs projectile-surface distance. (b) Population of shells with principal quantum numbers $n = 8-13$.

At the critical distance $R_c \approx 26$ a.u. capture into $n = 13$ starts, and soon AL permits population of $n = 12$ [Fig. 8(b)]. At $R \approx 21$ a.u., the lowering of the potential barrier and IS of the $n = 12$ shell permits RN to proceed into it, the result of which is that six electrons will quickly be captured. The increased population of $n = 12$ screens the nuclear charge for electrons in $n = 13$, and eventually at $R \approx 18$ a.u., causes their promotion into vacuum [Fig. 8(a)]. These parallel processes continue for the $n = 12$, 11, and 10 shells. We chose to stop our simulation at a distance of $R = 2$ a.u., because neither the concept of image charge nor the assumption of hydrogenic energy levels seems appropriate within a closer vicinity to a conducting surface.

From $R \approx 13$ a.u. on, the initial Ar^{12+} projectile remains practically neutralized [Fig. 8(a)], but carries all its captured electrons in highly excited states up to the moment of impact, where 12 electrons will still be residing in the states $n = 8$ through $n = 11$ [cf. Fig. 9(a)]. All these electrons are now peeled off, because the condition $r_B \leq \lambda_s$ permits only electrons with quantum numbers

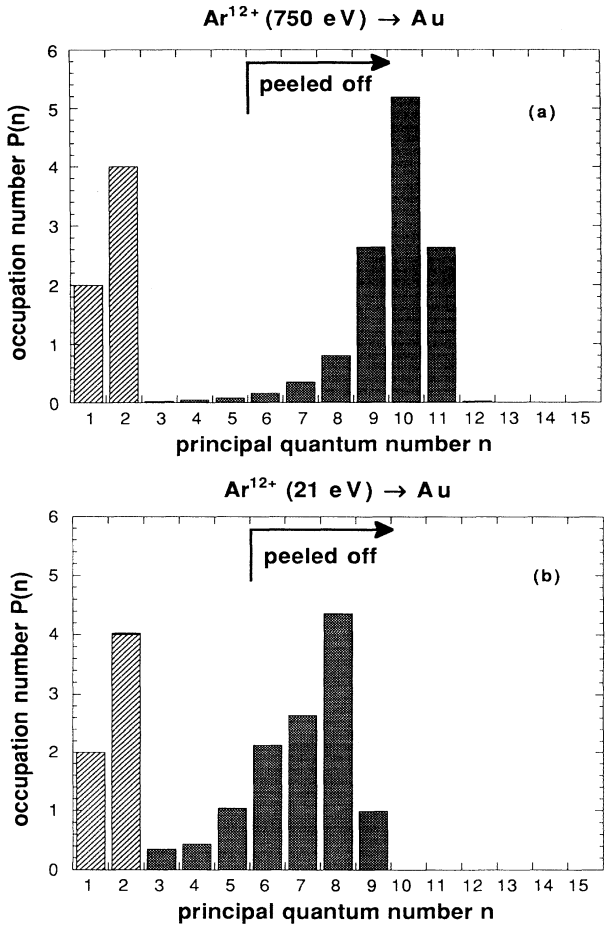

FIG. 9. Electron population of a hollow Ar atom resulting from neutralization or deexcitation of an Ar^{12+} having approached a gold surface to a distance of 2 a.u., for two different nominal kinetic energies.

$n < 6$ to remain in bound projectile states inside the solid. Only for initial projectile velocities $v_p \leq 10^4$ m/s [21 eV Ar^{12+}, Fig. 9(b)] there will be enough time for some electrons to reach the M and N shells. Our model calculations deliver a gain in kinetic energy of ~ 50 eV for Ar^{12+} due to its image charge acceleration, in good agreement with the value of 60 eV reported for scattering of the Xe^{12+} on a Fe(110) single-crystal surface [16]. Within the framework of the CBM model, the case illustrated in Fig 9(b) represents a lower limit to the accessible range of impact velocities imposed by image-charge acceleration and thus also a limit to the degree of deexcitation that can be reached by an AI cascade. This is supported by the observation that only a small fraction of fast Auger electrons can be emitted above the surface [10,43,44].

The now peeled off 12 electrons will of course be replaced within the solid almost instantaneously via processes like resonant capture of bulk core electrons or Auger neutralization by electrons from the conduction band. Very likely, a new, rather short-lived multiply excited atom will be formed with its electrons now captured into $n < 6$ shells, giving rise to fast inner-shell transitions, resulting in energetic Auger electron and/or x-ray photon emission, as reported in Refs. [2,10,13,43,44]. Such subsurface fast-Auger-electron-emission processes will be of no further concern in the present context, however.

In Fig. 10 the impact velocity dependence of the total electron emission as predicted by the CBM model has been compared with that of the measured total yields for impact of Ar^{12+} on gold (full symbols, cf. also Fig. 3). Note again that kinetic emission (KE) is negligibly small in the present velocity range.

The dashed curves indicate contributions of the three electron-emitting processes as regarded above. Peeling off together with SS+IS promotion provide a nearly velocity-independent contribution. To derive the total yields one simply has to add up the three contributions, but the result, labeled [$\Sigma 1$=(AI)+(PO)+(SS or IS)], obviously overestimates the measured yields. Some of the electrons emitted from the projectile into the 2π solid angle towards the surface may be absorbed by the metal, others will be reflected. Especially faster electrons may produce some secondary electrons. To our knowledge there are no reliable experimental data on reflection and secondary electron emission coefficients due to the impact of primary electrons in the 1–5-eV energy range, and we thus made two simple attempts to account "realistically" for these phenomena. For results denoted by $\Sigma 2$ it was assumed that all electrons promoted or peeled off can leave the surface, whereas only 50% of the AI electrons will be emitted towards the detector [$\Sigma 2$=(PO)+(SS or IS)+0.5(AI)]. On the other hand, by $\Sigma 1 \times 0.7$ we have denoted a situation where 30% of all electrons emitted by the projectile will be absorbed by the target metal. Both assumptions—however arbitrary—lead to surprisingly good agreement with the experimental data. Good agreement was found as well for the charge states $q = 10$, 14 and 16, whereas for $q < 8$ our model predictions and the experimental results disagreed by up to a factor of 2, which is probably caused by our too simple assumptions on the structure of electronic projectile levels involved.

Figure 11(a) illustrates that all three contributions to the modeled yield increase more or less linearly with the

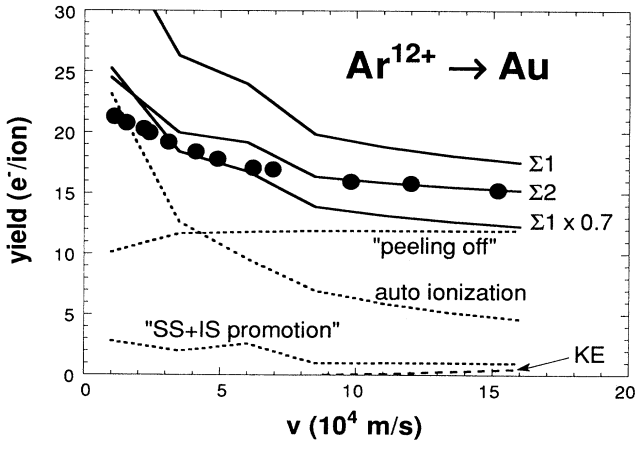

FIG. 10. Total electron emission yields for impact of Ar^{12+} on gold vs projectile velocity: Full symbols are measured yields. Contributions of different emission mechanisms are indicated by dashed lines. The total yields as derived under different assumptions are indicated by solid lines.

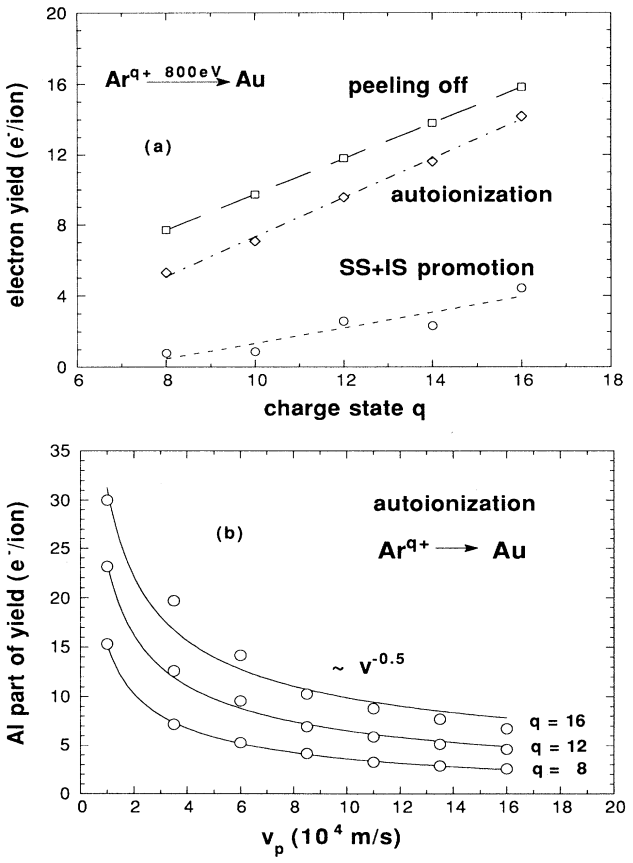

FIG. 11. (a) Contributions of the different emission mechanisms in the CBM model increase linearly with the projectile charge state q. (b) AI part of modeled total yield vs projectile nominal velocity, with a $v^{-1/2}$ curve fitted to the three sets of data points.

projectile charge state q. Of course any weighted sum of these contributions will also remain linear in q, in excellent agreement with the behavior of both the measured total yields and the fitting parameter γ_∞ resulting from Eq. (2) [cf. Fig. (6)]. The velocity dependence of the AI part of the total yield [Fig. 11(b)] can be described quite well by a $v^{-0.5}$ curve, again in good agreement with our measurements and the empirical formula [Eq. (2)]. The CBM simulations thus corroborate our initial assumption [29], that the total electron emission yields are composed of two contributions, only one of them depending on the projectile impact velocity v_p, and identify this contribution to result from AI electron emission. The rest of the electrons contributing to the measured total yields seems to depend only rather weakly on v_p, and can be explained by IS+SS promotion during the approach of the projectile to the surface and by peeling off upon surface impact, respectively.

Finally, we found our model to be rather insensitive to the only source term in the system (i.e., RN), since the latter could be varied by up to a factor of 5 without any crucial changes for the evolution of the electronic population of the approaching projectile. We therefore conclude that within the framework of the CBM model, mainly the height of the barrier (which "opens" and "closes" the channel for RN) determines where and how many electrons are captured, whereas other parameters like the current density of captured electrons or the topology of the potential surface do not seem to restrict RN, once over-the-barrier capture has become possible. Variation of the assumed AI rates, however, will change not only the number of emitted Auger electrons, but also the number of electrons subject to both SS+IS promotion and peeling off, because both mechanisms depend on the distribution of electrons over the different projectile shells, i.e., how far the AI cascade has already progressed.

Of course the projectile's evolution predicted by the calculations is much more detailed than can (or probably ever will) be deduced from the experimental information and the scenario presented is neither unique nor complete. For example, emission of slow electrons due to subsurface processes has been neglected completely but might play a non-negligible role. Since the calculated results agree in velocity dependence as well as charge-state dependence and (within certain limits) even in absolute magnitude with our experiment, we believe that our scenario is a rather reasonable one, although refinements might be necessary in the light of future experience.

V. CONCLUSIONS

An innovative technique of measuring electron-emission statistics, combined with production of rather slow MCI by means of a recoil-ion source, has been applied to determine rather precise total electron yields for very low fluxes of highly charged projectiles. This method seems to be almost ideally suited to study electron emission from ions in higher charge states impinging perpendicularly on a metal surface with rather low kinetic energy. In this way the slow electrons, which constitute the overwhelming part of all electrons emitted, can be detected almost completely.

We applied a classical over-the-barrier model to describe the dynamics of neutralization, deexcitation, and electron emission during the MCI approach toward a clean gold surface. Despite some crude simplification inherent in this model, comparison with the experimental data is rather successful and thus permits quite realistic estimates for the involved time scales and relative efficiencies of electron emitting processes. Furthermore, our simulations suggest the processes of IS+SS promotion and peeling off to be responsible for those slow electrons that are emitted almost independent of the projectile's velocity, as they cannot result from autoionization-cascades during the projectile's approach toward the surface.

ACKNOWLEDGMENTS

The authors acknowledge important contributions of Dr. R. Mann (GSI Darmstadt) by participating in the experimental work, and also the kind support of other colleagues from GSI who provided an excellent working environment. Furthermore, they thank Professor J. Burgdörfer (University of Tennessee, Knoxville) for valuable discussions on the applicability of his CBM model. This work has been supported by Austrian Fonds zur Förderung der wissenschaftlichen Forschung (Project No. P8315TEC), and by Kommission zur Koordination der Kernfusionsforschung at the Austrian Academy of Sciences.

[1] E. D. Donets, Phys. Scr. **T3**, 11 (1983).
[2] J. P. Briand, L. de Billy, P. Charles, S. Essabaa, P. Briand, R. Geller, J. P. Desclaux, S. Bliman, and C. Ristori, Phys. Rev. Lett. **65**, 159 (1990); Phys. Rev. A **43**, 565 (1991).
[3] D. M. Zehner, S. H. Overbury, C. C. Havener, F. W. Meyer, and W. Heiland, Surf. Sci. **178**, 359 (1986).
[4] S. T. de Zwart, Ph.D. thesis, Rijksuniversiteit Groningen (1987).
[5] L. Folkerts, Ph.D. thesis, Rijksuniversiteit Groningen (1992) and references therein to work of other groups.
[6] H. D. Hagstrum, Phys. Rev. **96**, 325 (1954); **96**, 336 (1954).
[7] M. Delaunay, M. Fehringer, R. Geller, D. Hitz, P. Varga, and HP. Winter, Phys. Rev. B **35**, 4232 (1987).
[8] U. A. Arifov, E. S. Mukhamadiev, E. S. Parilis, and A. S. Pasyuk, Zh. Tekhn. Fiz. **43**, 375 (1973) [Sov. Phys. Tech. Phys. **18**, 240 (1973)].
[9] R. Köhrbrück, K. Sommer, J. P. Biersack, J. Bleck-Neuhaus, S. Schippers, P. Roncin, D. Lecler, F. Fremont, and N. Stolterfoht, Phys. Rev. A **45**, 4653 (1992).
[10] H. J. Andrä *et al.*, in *Proceedings of the XVIIth International Conference on the Physics of Electronic and Atomic Collisions,* edited by W. R. MacGillivray, I. E. McCarty, and M. C. Standage (IOP Conference Proceedings, Brisbane, 1991), p. 89.
[11] S. T. de Zwart, A. G. Drentje, A. L. Boers, and R. Morgenstern, Surf. Sci. **217**, 298 (1989).
[12] P. A. Zeijlmans van Emmichoven, C. C. Havener, and F. W. Meyer, Phys. Rev. A **43**, 1405 (1991).
[13] F. W. Meyer, S. H. Overbury, C. C. Havener, P. A. Zeijlmans van Emmichhoven, J. Burgdörfer, and D. M.

Zehner, Phys. Rev. A **44**, 7214 (1991).
[14] S. T. de Zwart, T. Fried, U. Jellen, A. L. Boers, and A. G. Drentje, J. Phys. B. **18**, L623 (1985).
[15] H. Winter, Europhys. Lett. **18**, 207 (1992).
[16] H. Winter, in *Proceedings of the Sixth International Conference on the Physics of Highly Charged Ions* (Manhattan, Kansas, 1992), edited by P. Richard *et al.*, AIP Conf. Proc. No. 274 (AIP, New York, 1993), p. 583.
[17] E. D. Donets, Nucl. Instrum. Methods. Phys. Res. Sect. B **9**, 522 (1985).
[18] M. Schulz, C. L. Cocke, S. Hagmann, M. Stöckli, and H. Schmidt-Böcking, Phys. Rev. A **44**, 1653 (1991).
[19] M. Delaunay, M. Fehringer, R. Geller, P. Varga, and H. P. Winter, Europhys. Lett. **4**, 377 (1987).
[20] J. W. McDonald, D. Schneider, M. W. Clark, and D. Dewitt, Phys. Rev. Lett. **68**, 2297 (1992).
[21] L. Folkerts and R. Morgenstern, Europhys. Lett. **13**, 377 (1990).
[22] P. Varga, Comments At. Mol. Phys. **27**, 111 (1989).
[23] H. P. Winter, Z. Phys. D **21**, S129 (1991).
[24] P. Varga and H. P. Winter, in *Particle Induced Electron Emission II,* edited by G. Höhler (Springer, Heidelberg, 1992), Vol. 123.
[25] J. Burgdörfer, P. Lerner, and F. W. Meyer, Phys. Rev. A **44**, 5674 (1991); J. Burgdörfer and F. W. Meyer, *ibid.* A **47**, R20 (1993).
[26] J. N. Bardsley and B. M. Penetrante, Comments At. Mol. Phys. **27**, 43 (1991).
[27] U. Wille, Phys. Rev. A **45**, 3004 (1992).
[28] N. Vaeck and J. E. Hansen, J. Phys. B **24**, L469 (1991).
[29] H. Kurz, K. Töglhofer, HP. Winter, F. Aumayr, and R. Mann, Phys. Rev. Lett. **69**, 1140 (1992).
[30] S. Kelbch, J. Ullrich, R. Mann, P. Richard, and H. Schmidt-Böcking, J. Phys. B **18**, 323 (1985).
[31] R. E. Olson, J. Ullrich, and H. Schmidt-Böcking, J. Phys. B **20**, L809 (1987).
[32] G. Lakits, F. Aumayr, M. Heim, and HP. Winter, Phys. Rev. A **42**, 5780 (1990).
[33] G. Lakits, F. Aumayr, and HP. Winter, Rev. Sci. Instrum. **60**, 3151 (1989).
[34] H. Drescher, L. Reimer, and H. Seidel, Z. Angew. Phys. **29**, 331 (1979).
[35] H. Kulenkampff and W. Spyra, Z. Phys. **137**, 416 (1954).
[36] W. K. van Asselt, B. Poelsema, and A. L. Boers, J. Phys. D **11**, L107 (1978).
[37] F. Aumayr, G. Lakits, and HP. Winter, Appl. Surf. Sci. **47**, 139 (1991).
[38] K. Töghofer, F. Aumayr, and HP. Winter, Surf. Sci. **281**, 143 (1993).
[39] J. C. Slater, Phys. Rev. **36**, 57 (1930).
[40] R. L. Kelly and L. J. Palumbo (unpublished).
[41] G. Betz (private communication).
[42] J. Müller and J. Burgdörfer, Phys. Rev. A **43**, 6027 (1991).
[43] F. W. Meyer, S. H. Overbury, C. C. Havener, P. A. Zeijlmans van Emichhoven, and D. M. Zehner, Phys. Rev. Lett. **67**, 723 (1991).
[44] J. Das and R. Morgenstern, in *Proceedings of the Sixth International Conference on the Physics of Highly Charged Ions* (Ref. [16]), p. 563.